Comparison of Dual-Head Coincidence Gamma Camera FDG Imaging with FDG PET in Detection of Breast Cancer and Axillary Lymph Node Metastasis

Kenji Yutani, Mitsuaki Tatsumi, Eiichi Shiba, Hideo Kusuoka and Tsunehiko Nishimura

Divisions of Tracer Kinetics and Oncological Surgery, Biomedical Research Center, Osaka University Medical School, Osaka, Japan

Dual-head coincidence gamma camera ^{18}F-fluorodeoxyglucose (FDG) imaging was compared with FDG PET in the detection of breast cancer and axillary lymph node metastasis. **Methods:** Both coincidence gamma camera FDG imaging and FDG PET were performed in a cylindrical phantom containing spheres of different sizes and activity ratios (5:1, 10:1 and 15:1) and in 30 women (age range 32–78 y) with suspected breast cancer. Biopsies or mastectomies were performed in all patients. Images were visually assessed, and the count ratio between tumor and normal tissue (T/N ratio) was calculated. **Results:** In the phantom studies, coincidence gamma camera imaging visualized the smallest sphere (1.0 cm) at a ratio of 15:1 but not at ratios of 5:1 and 10:1. Coincidence gamma camera imaging visualized the other spheres (≥1.3 cm) at all ratios. PET visualized all spheres at all ratios. In the clinical studies, 22 of 26 breast carcinomas detected by PET were also detected by coincidence gamma camera imaging. Coincidence gamma camera imaging detected all of the carcinomas ≥2 cm in diameter (n = 10) and 12 of 16 carcinomas <2 cm. In breast carcinomas detected by both PET and coincidence gamma camera imaging, the T/N ratio in non–attenuation-corrected PET (7.12 ± 7.13) was significantly higher than in coincidence gamma camera imaging (2.90 ± 1.47, $P < 0.005$). Four of 8 axillary lymph node metastases detected by PET were detected by coincidence gamma camera imaging. Of 9 axillary lymph node metastases <1.0 cm in diameter, 7 and 3 were detected by PET and coincidence gamma camera imaging, respectively. **Conclusion:** Coincidence gamma camera imaging is useful in detecting breast carcinoma ≥2 cm in diameter but is not reliable for breast carcinoma <2 cm in diameter. Coincidence gamma camera imaging may be useless or even dangerous in the detection of axillary lymph node metastasis.

Key Words: breast cancer; axillary lymph node metastasis; PET; dual-head coincidence imaging; fluorodeoxyglucose

J Nucl Med 1999; 40:1003–1008

Breast cancer is a major disease afflicting women in affluent countries (*1*). The incidence of breast cancer has been steadily increasing in the U.S. The most common modality for detecting breast cancer is mammography, which is very sensitive but has a low positive predictive value (*2*). Furthermore, mammography cannot always visualize breast tumors in patients with dense breast tissue. A reliable technique is required to differentiate benign from malignant breast tumors and to overcome the limitations imposed by the low positive predictive value of mammography. One of the most important prognostic factors in patients with breast cancer is metastasis to axillary lymph nodes (*3*). Axillary dissection can locally control such metastasis. However, because of the widespread use of adjuvant systemic therapy, the principal purpose of axillary dissection is often simply to provide prognostic information (*4*). In addition, axillary lymph node dissection is associated with complications such as wound infection, seroma formation, shoulder dysfunction and lymphedema of the ipsilateral arm (*5*). An effective noninvasive procedure is therefore required to detect axillary lymph node metastasis.

PET with ^{18}F-fluorodeoxyglucose (FDG) has been used to detect breast cancer and axillary lymph node metastasis (*6–14*). The sensitivity of FDG PET for primary breast cancer varies between 68% and 100%, and that for axillary lymph node metastasis varies between 79% and 100%. In some countries, however, the limited number of PET centers precludes PET studies for all patients with suspicious lesions. SPECT is one alternative to PET. There are two techniques for using the SPECT system to image the 511-keV photons of positron emitters, one with an ultra-high-energy collimator (UHC) and the other with the SPECT system in coincidence mode (coincidence gamma camera imaging). The latter technique has higher spatial resolution and sensitivity but is degraded by a higher proportion of scatter and random coincidence events in the reconstructed images (*15*). Several studies have demonstrated the usefulness of FDG SPECT with UHC to visualize malignancies

Received Jul. 7, 1998; revision accepted Nov. 30, 1998.

For correspondence or reprints contact: Tsunehiko Nishimura, MD, PhD, Division of Tracer Kinetics, Osaka University Medical School, 2-2 Yamadaoka, Suita Osaka 565-0871 Japan.

(*16–23*). In this study, we compared the abilities of coincidence gamma camera imaging and PET to detect primary breast tumors and axillary nodal metastases.

MATERIALS AND METHODS

Coincidence gamma camera images were obtained with a dual-head gamma camera (Vertex MCD; ADAC Laboratories, Milpitas, CA). The in-plane spatial resolution was 4.8 mm full width at half maximum (FWHM) at the center of the field of view, with an axial field of view of 38 cm. In the transverse direction, the spatial resolution was largely constant radially as well as tangentially at any distance from the center toward the edge of a transverse slice. There was a slight (+10%) degradation as the distance from the center increased. In the axial direction, the spatial resolution (FWHM) was about twice that of the transverse. The greatest sensitivity of the system was 2.7 cps/Bq/cm^3, which was measured at the center between the two detectors. From the center, the sensitivity decreased linearly in any direction, axially or transversely, until it reached zero at points on the planes connecting the edges of the field of view of the two detectors. PET images were obtained with a Shimadzu Headtome V (SET-2000W; Shimadzu Co., Kyoto, Japan). The PET camera was operated in the two-dimensional mode. It had an in-plane spatial resolution of 4.0 mm FWHM and an axial resolution of 4.5 mm FWHM at the center of the field of view. The axial and transverse fields of view were 20 and 51 cm, respectively. The sensitivity was 7.3 cps/Bq/cm^3. The spatial resolution and sensitivity of the coincidence gamma camera and the PET camera were measured according to the standard National Electrical Manufacturers Association procedure.

Phantom Study

To evaluate the performance of the coincidence gamma camera imaging and PET, a 20-cm-diameter cylindrical phantom containing six spheres of inside diameters of 1.0–3.8 cm was imaged. The axial length of the phantom was 20 cm. The wall thickness of the spheres was 2 mm. Both the phantom and spheres were filled with a solution that contained ^{18}F-FDG. Three acquisitions were performed with the concentrations adjusted to provide a ratio of sphere-to-background activity of 5:1, 10:1 or 15:1. ^{18}F-FDG activity in the background solution was 4700 Bq/mL. The equivalent standardized uptake value (SUV) of the background activity in a typical patient (60 kg) at 1 h postinjection of 370 MBq was 1.1. For PET, emission scanning was performed for 20 min. Subsequently, the phantom was scanned by the coincidence gamma camera with a 128 × 128 matrix, 180° rotation, 32 steps and an acquisition time of 50 s per step.

PET data were reconstructed both with and without geometric attenuation correction, in a 128 × 128 matrix, with a filter obtained by multiplying a ramp filter by a Butterworth filter (cutoff frequency 0.083 cycles/mm). The coincidence gamma camera imaging data were also reconstructed both with and without geometric attenuation correction by means of filtered backprojection methods with a Wiener filter (cutoff frequency 0.14 cycles/mm, order of 1). Circular regions of interest (ROIs), the size of the smallest sphere, were defined over spheres and over a background area in attenuation-corrected images for both PET and coincidence gamma camera imaging, and contrast ratios of measured sphere counts to background counts were calculated.

Clinical Study

Patients. We studied 30 women out of 84 consecutive patients (age range 32–78 y, average age 51 y) who were referred to the breast cancer clinic of our hospital between April 1997 and April 1998 because of suspicion of breast cancer. Each breast lesion was detected by physical examination or mammography. Patients were first selected randomly on the basis of the availability of PET and coincidence gamma cameras. Then, the patients who gave written, informed consent were enrolled in this study. PET and coincidence gamma camera imaging were performed on the same day. Serum glucose level of the all patients was determined at the time of ^{18}F-FDG injection. None of the patients had diabetes. All patients underwent excisional biopsy or mastectomy within 5 d of the imaging procedures. In addition, all patients with breast cancer underwent axillary dissection.

Imaging Procedures. All patients fasted for at least 4 h before the start of the study. For PET, transmission scan was performed for 10 min. Sixty minutes after intravenous administration of 370 MBq ^{18}F-FDG, emission scanning was performed for 20 min. Approximately 2 h after PET scanning (range 1.8–2.5 h, average 2.1 h), coincidence gamma camera imaging was performed using a dual-head gamma camera with a 128 × 128 matrix, with energy windows of 511 keV ± 15%, 180° rotation, 32 steps and an acquisition time of 50 s per step. PET data were reconstructed both with and without attenuation correction, in a 128 × 128 matrix, with a filter obtained by multiplying a ramp filter by a Butterworth filter (cutoff frequency 0.083 cycles/mm). The coincidence gamma camera imaging data were reconstructed by filtered backprojection methods with a Wiener filter (cutoff frequency 0.14 cycles/mm, order of 1).

The tracer was administered into the antecubital vein of the arm on the side contralateral to the breast with the suspected tumor. Patients were scanned in the supine position with their arms above their heads.

Data Analysis. Tumor images were visually assessed by two independent observers who had no knowledge of pathological findings. For visual interpretation, a positive lesion was defined as any activity above local background. The count ratio of tumor to that of normal tissue (T/N ratio) was calculated in both PET and coincidence gamma camera images. The tumor count was measured at the ROI set on the area corresponding to the breast tumor. The normal count was obtained by setting an ROI on the contralateral normal breast. In PET images, the SUV was also calculated (*24*):

$$\text{SUV} = \text{tissue activity (Bq/g)} \,/\, [\text{injected dose (Bq)} \,/\, \text{body weight (g)}].$$

Statistical Analysis. Data are expressed as mean ± SD. Statistical significance was determined using Student t test for paired data. $P < 0.05$ was considered significant.

RESULTS

Phantom Study

Figure 1 shows the phantom images with the hot spheres at a ratio of 5:1, both with and without geometric attenuation correction. Measured contrast ratios calculated for the hot lesions in a warm background are shown in Figure 2. The result of lesion detection in attenuation-corrected coincidence gamma camera images was equal to that in noncorrected ones. The same was true of PET images. The effect of attenuation was much greater in coincidence gamma camera imaging than in PET. Coincidence gamma camera imaging

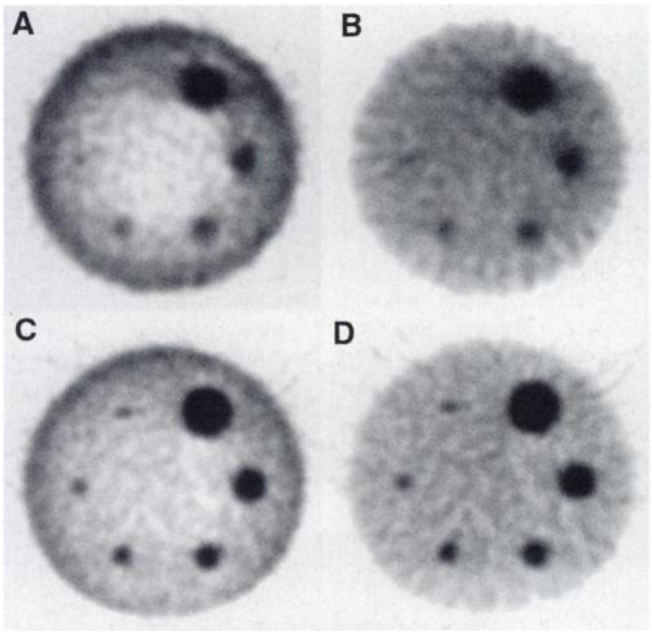

FIGURE 1. Phantom images with hot spheres at ratio of 5:1. (A) Coincidence gamma camera (CGC) without attenuation correction (AC). (B) CGC with geometric attenuation correction (GAC). (C) PET without AC. (D) PET with GAC. ^{18}F-FDG activity in background solution was 4700 Bq/mL. Equivalent SUV of background activity in typical patient (60 kg) at 1 h postinjection of 370 MBq was 1.1.

visualized the smallest sphere (1.0 cm) at a ratio of 15:1 but not at ratios of 5:1 and 10:1. The other spheres (≥1.3 cm) were visualized at all ratios by coincidence gamma camera imaging. PET visualized all spheres at all ratios, yielding

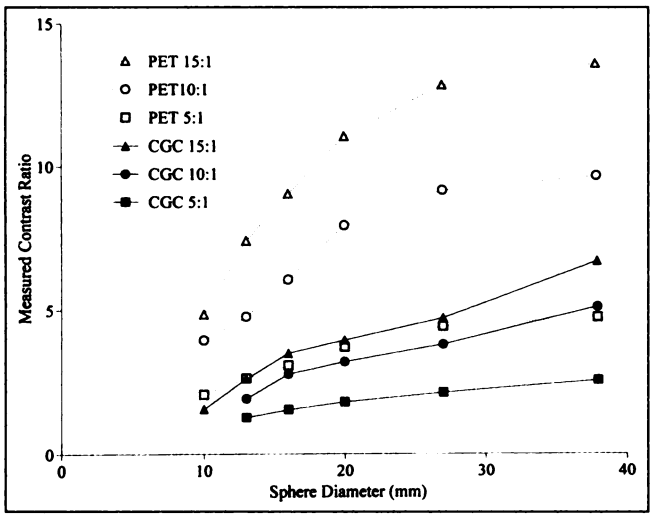

FIGURE 2. Targets (spheres)-to-background ratios with coincidence gamma camera (CGC) and PET are plotted against diameters of spheres (1.0–3.8 cm). Data of both modalities were reconstructed with geometric attenuation correction. Activity of ^{18}F-FDG in targets and background was adjusted to provide ratios of 5:1, 10:1 and 15:1. Because smallest sphere (1.0 cm) with ratios of 5:1 and 10:1 was not visualized by CGC imaging, data were not plotted.

significantly better results than those obtained with coincidence gamma camera imaging ($P < 0.005$).

Clinical Study

The patient data are summarized in Table 1. Breast cancer was confirmed in 26 patients, and the other 4 had benign lesions. Mean size of the primary breast carcinomas was 1.9 cm in diameter (range 0.9–3.8 cm). Mammography detected 28 breast tumors, of which 9 were indeterminate and 19 were mammographically malignant.

Twenty-two of the breast carcinomas were detected by coincidence gamma camera imaging, and all 26 carcinomas were detected by PET. Two benign breast tumors (1 phyllodes tumor and 1 intraductal papilloma) were visualized by both modalities. Neither coincidence gamma camera imaging nor PET visualized the 2 cases of fibrocystic disease. The result of the blinded visual interpretation of non–attenuation-corrected PET images was equal to that of attenuation-corrected ones. The sensitivity and accuracy of coincidence gamma camera imaging were 84.6% and 80.0%, respectively, and those of PET were 100% and 93.3%, respectively. The specificity, positive predictive value and negative predictive value were not calculated, because the number of patients with benign breast lesions (n = 4) was insufficient. Coincidence gamma camera and attenuation-corrected images of a patient with right breast cancer are shown (Fig. 3).

The relationship between tumor size and T/N ratio is summarized in Figure 4. All cases of breast cancer (n = 26) were plotted. Coincidence gamma camera imaging detected all breast carcinomas >1.8 cm in diameter. The diameter of the smallest breast carcinoma detected by coincidence gamma camera imaging was 0.9 cm. Of 4 breast carcinomas that were not detected by coincidence gamma camera imaging, 1 was small (1 cm in diameter, Fig. 5), and the other 3 showed low T/N ratios on PET images (1.30, 1.42 and 1.50). In breast carcinomas detected by both PET and coincidence gamma camera imaging (n = 22), the T/N ratio in non–attenuation-corrected PET (7.12 ± 7.13) was significantly higher than that in coincidence gamma camera imaging (2.90 ± 1.47, $P < 0.005$). The difference between the T/N ratio in attenuation-corrected PET (6.09 ± 5.24) and that in non–attenuation-corrected PET was not significant.

Of 26 patients with breast cancer, 10 had axillary lymph node metastasis. Table 2 summarizes the data on axillary lymph nodes. There were no false-positive results with either coincidence gamma camera imaging or PET examination in detection of axillary lymph node metastasis. Coincidence gamma camera imaging detected 4 of 8 axillary lymph node metastases that were detected by PET. PET detected all axillary lymph node metastases when the diameter of the largest metastatic lymph node was ≥5 mm. All of the axillary lymph node metastases ≥9 mm were detected by coincidence gamma camera imaging. The diameters of the smallest lymph node detected by coincidence gamma camera imaging and PET were 7 and 5 mm, respectively. Thus, PET was more sensitive than coinci-

TABLE 1
Summary of Data on Breast Masses

Patient no.	Age (y)	Size of lesion (cm)	Pathology	Clinical findings	Mammographic findings	CGC T/N	PET non-AC T/N	PET AC T/N	PET SUV
1	52	3.8	Invasive ductal ca	Palp	Prob malignant	1.82	2.66	2.08	1.09
2	55	3.0	Invasive ductal ca	Palp	Prob malignant	4.91	4.58	7.71	2.59
3	42	2.9	Invasive ductal ca	Palp	Indeterminate	4.06	13.21	10.89	3.07
4	78	2.4	Invasive ductal ca	Palp	Prob malignant	3.30	6.82	5.62	2.62
5	47	2.3	Invasive ductal ca	Palp	Prob malignant	1.99	2.11	3.27	1.58
6	38	2.3	Invasive ductal ca	Palp	Prob malignant	2.88	4.34	4.56	1.64
7	43	2.2	Invasive ductal ca	Palp	Prob malignant	4.33	6.83	5.78	5.90
8	49	2.2	Invasive ductal ca	Palp	Prob malignant	2.51	3.27	5.60	2.85
9	69	2.1	Invasive ductal ca	Palp	Prob malignant	6.07	22.81	19.91	5.78
10	32	2.1	Invasive ductal ca	Palp	Prob malignant	3.45	14.71	7.04	2.61
11	50	1.8	Invasive ductal ca	Palp	Indeterminate	1.41	2.62	1.65	1.36
12	54	1.8	Invasive ductal ca	Palp	Prob malignant	2.12	4.32	4.24	1.96
13	58	1.7	Invasive ductal ca	Palp	Indeterminate	6.37	30.27	20.23	0.66
14	41	1.6	Invasive ductal ca	Palp	Prob malignant	1.55	3.91	3.06	2.11
15	74	1.6	Invasive ductal ca	Palp	Prob malignant	1.41	2.27	1.83	0.98
16	72	1.5	Invasive ductal ca	Palp	Indeterminate	neg	2.58	1.42	1.09
17	33	1.4	Invasive ductal ca	Palp	Prob malignant	2.69	4.82	4.74	2.12
18	65	1.4	Invasive ductal ca	Palp	Indeterminate	1.96	2.22	2.61	1.70
19	42	1.4	Invasive ductal ca	Palp	Indeterminate	1.36	1.56	1.61	1.04
20	60	1.2	Invasive ductal ca	Palp	Prob malignant	4.10	11.01	12.76	2.44
21	46	1.1	Invasive ductal ca	Palp	Prob malignant	1.99	4.98	2.83	1.48
22	46	1.1	Invasive ductal ca	Palp	Prob malignant	2.11	4.20	4.02	2.14
23	66	1.0	Invasive ductal ca	Palp	Prob malignant	neg	4.04	3.44	1.50
24	53	0.9	Invasive ductal ca	Palp	No lesion	1.31	3.11	2.02	0.96
25	50	1.8	Medullary ca	Palp	Prob malignant	neg	1.82	1.30	0.70
26	50	1.7	Invasive lobular ca	Palp	No lesion	neg	2.85	1.50	1.07
27	37	3.7	Phyllodes tumor	Palp	Indeterminate	3.03	4.22	3.31	1.81
28	47	1.1	Intraductal papilloma	Palp	Indeterminate	1.81	5.08	4.70	2.28
29	44	—	Fibrocystic disease	Nonpalp	Prob malignant	neg	neg	neg	—
30	33	—	Fibrocystic disease	Palp	Indeterminate	neg	neg	neg	—

CGC = coincidence gamma camera; T/N = tumor-to-normal tissue ratio; AC = attenuation correction; SUV = standardized uptake value; ca = carcinoma; Palp = palpable; Prob = probably; neg = negative scan; — = not measurable.

dence gamma camera imaging in detecting axillary lymph node metastases (80.0% and 40.0%, respectively). The specificities and positive predictive values of both procedures were 100%. The accuracies and negative predictive values of coincidence gamma camera imaging were 76.9% and 72.7%, respectively, and those of PET were 92.3% and 88.9%, respectively.

DISCUSSION

In clinical oncology, ^{18}F-FDG imaging has been reported to provide important diagnostic information not obtained by morphological imaging modalities (*25*). PET imaging is the most suitable means of acquiring ^{18}F-FDG images. Recently, attempts have been made to acquire ^{18}F-FDG images using a

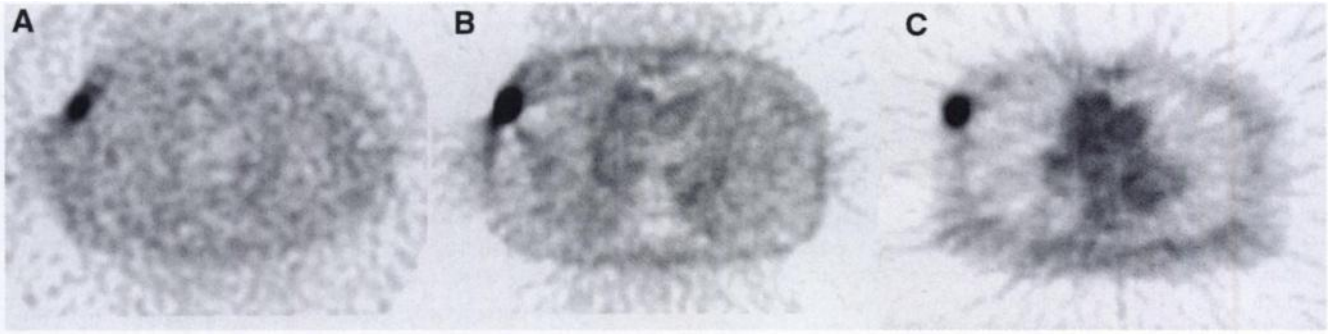

FIGURE 3. Coincidence gamma camera (A), non–attenuation-corrected PET (B) and attenuation-corrected PET (C) images of invasive ductal carcinoma in right upper outer quadrant of breast of 78-y-old woman (patient 4). Tumor was 2.4 cm in diameter. SUV of breast carcinoma was 2.62. High uptakes of ^{18}F-FDG were observed in right breast carcinoma in all three images.

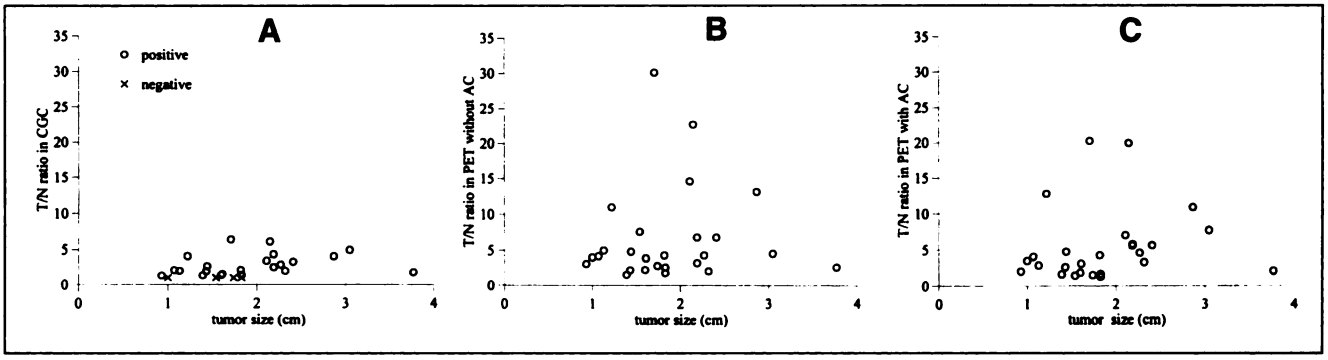

FIGURE 4. Relationship between tumor size and T/N ratio. Circles and crosses represent positive and negative findings, respectively. (A) Coincidence gamma camera (CGC) imaging. (B) PET without attenuation correction (AC). (C) PET with AC.

SPECT camera. According to previous reports, FDG SPECT with UHC may not be able to detect tumors <2 cm (*18–21,23*). Holle et al. (*20*) reported that FDG SPECT with UHC accurately detected all breast carcinomas >2.3 cm, and the smallest FDG-positive lesion was 1.4 cm. For tumors <2 cm, they showed that FDG SPECT with UHC accurately detected 4 of 11 breast carcinomas (36.4%). In this study, all breast carcinomas >1.8 cm were detected by coincidence gamma camera imaging, and the smallest true-positive lesion was 0.9 cm. Moreover, coincidence gamma camera imaging detected 12 of 16 breast carcinomas (75.0%) <2 cm. These results indicate that coincidence gamma camera imaging may be superior to SPECT with UHC in the detection of breast cancer.

In this study, coincidence gamma camera imaging detected all of the breast carcinomas ≥2 cm (n = 10) and 12 of 16 carcinomas <2 cm, whereas PET detected all 26 carcinomas. These results suggest that coincidence gamma camera imaging is useful in detecting breast cancer ≥2 cm but is not reliable for breast cancer <2 cm in diameter because of the high rate of false-negatives. On the other hand, only half of the axillary lymph node metastases detected by FDG PET were detected by coincidence gamma camera imaging. As shown in Tables 1 and 2, the axillary lymph node metastases were clearly smaller than breast tumors. Of 9 axillary lymph node metastases <1.0 cm, PET and coincidence gamma camera imaging detected 7 (77.8%) and 3 (33.3%), respectively. Coincidence gamma camera imaging may be useless or even dangerous in the detection of axillary lymph node metastasis.

The T/N ratios in both phantom and clinical studies were significantly greater in PET than in coincidence gamma camera imaging. Because coincidence gamma camera imaging operates in a three-dimensional mode, substantial nontrue coincidences occur because of the increase in both random and scatter coincidence (*26*). Moreover, the counting rate capability of the gamma camera in coincidence mode is limited. These factors may chiefly contribute to the lower T/N ratios in coincidence gamma camera images.

The effect of attenuation is much greater in coincidence images than in PET images without attenuation correction, meaning that it may be difficult to differentiate a pathological uptake from a physiologic one in some cases (*15*). Therefore, coincidence gamma camera images without attenuation correction should be evaluated with caution. In this study, there was no difference in lesion detection between attenuation-corrected PET and uncorrected PET. Some investigators have reported similar observations (*27,28*). Thus, it is not clear whether addition of attenuation correction to coincidence images increases diagnostic accuracy in the detection of malignancies.

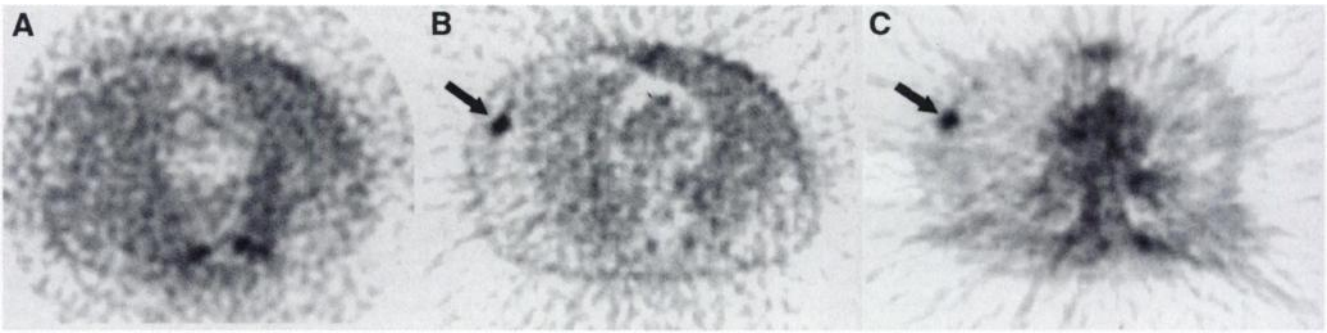

FIGURE 5. Coincidence gamma camera (CGC) (A), non–attenuation-corrected PET (B) and attenuation-corrected PET (C) images of invasive ductal carcinoma in right upper outer quadrant of breast of 66-y-old woman (patient 23). Tumor was 1.0 cm in diameter. SUV of breast carcinoma was 1.50. Uptake of ^{18}F-FDG in right breast carcinoma was clearly visualized by both attenuation-corrected and uncorrected PET (arrow), but CGC imaging could not detect uptake.

TABLE 2
Summary of Axillary Lymph Nodes in Patients with Metastasis

Patient no.	Axillary lymph nodes: Total no. sampled	No. metastatic	Maximum size metastatic (mm)	Clinical findings	CGC	PET
2	18	13	7	Palp	Pos	Pos
3	15	1	9	Nonpalp	Pos	Pos
4	10	3	7	Nonpalp	Neg	Pos
6	18	3	5	Nonpalp	Neg	Pos
8	19	2	9	Palp	Pos	Pos
12	13	1	3	Palp	Neg	Neg
13	18	2	16	Nonpalp	Pos	Pos
16	28	9	8	Palp	Neg	Pos
20	19	1	5	Nonpalp	Neg	Pos
26	13	4	4	Nonpalp	Neg	Neg

CGC = coincidence gamma camera; Palp = palpable; Pos = positive scan; Neg = negative scan.

In this study, a coincidence image was obtained approximately 2 h after PET scanning, because the counting rate capability of coincidence gamma camera imaging was limited (*15*). If we perform both examinations at the same time after administration of ^{18}F-FDG, a 2-d protocol is needed and the patient exposure is increased. The ^{18}F-FDG uptake ratio of tumor to background tissue has been reported to increase over time (*29*). Therefore, this study protocol might give coincidence gamma camera imaging an advantage over PET imaging.

CONCLUSION

Twenty-two of 26 breast carcinomas detected by PET were also detected by coincidence gamma camera imaging. Coincidence gamma camera imaging detected all of the carcinomas ≥2 cm in diameter (n = 10) and 12 of 16 carcinomas <2 cm. The T/N ratio in PET was significantly greater than that in coincidence gamma camera imaging in both phantom and clinical studies. Four of 8 axillary lymph node metastases detected by PET were detected by coincidence gamma camera imaging. Of 9 axillary lymph node metastases <1.0 cm, 7 and 3 were detected by PET and coincidence gamma camera imaging, respectively. These results indicate that coincidence gamma camera imaging is useful in detecting breast carcinomas ≥2 cm in diameter but is not reliable for breast carcinomas <2 cm in diameter. Coincidence gamma camera imaging may be useless or even dangerous in the detection of axillary lymph node metastasis.

REFERENCES

1. Harris JR, Lippman ME, Veronesi U, Willett W. Breast cancer (1). *N Engl J Med.* 1992;327:319–328.
2. Kopans DB. The positive predictive value of mammography. *AJR.* 1992;158:521–526.
3. Nemoto T, Vana J, Bedwani RN, Baker HW, McGregor FH, Murphy GP. Management and survival of female breast cancer: results of a national survey by the American College of Surgeons. *Cancer.* 1980;45:2917–2924.
4. Harris JR, Morrow M, Bonadonna G. Cancer of the breast. In: DeVita VT Jr, Hellman S, Rosenberg SA, eds. *Cancer: Principles and Practice of Oncology.* 4th ed. Philadelphia, PA: Lippincott; 1993:1264–1332.
5. Siegel BM, Mayzel KA, Love SM. Level I and II axillary dissection in the treatment of early-stage breast cancer. An analysis of 259 consecutive patients. *Arch Surg.* 1990;125:1144–1147.
6. Wahl RL, Cody RL, Hutchins GD, Mudgett EE. Primary and metastatic breast carcinoma: initial clinical evaluation with PET with the radiolabeled glucose analogue 2-[F-18]-fluoro-2-deoxy-D-glucose. *Radiology.* 1991;179:765–770.
7. Scheidhauer K, Scharl A, Pietrzyk U, et al. Qualitative [^{18}F]FDG positron emission tomography in primary breast cancer: clinical relevance and practicability. *Eur J Nucl Med.* 1996;23:618–623.
8. Avril N, Dose J, Jnicke F, et al. Metabolic characterization of breast tumors with positron emission tomography using F-18 fluorodeoxyglucose. *J Clin Oncol.* 1996;14:1848–1857.
9. Nieweg OE, Kim EE, Wong WH, et al. Positron emission tomography with fluorine-18-deoxyglucose in the detection and staging of breast cancer. *Cancer.* 1993;71:3920–3925.
10. Adler LP, Crowe JP, al-Kaisi NK, Sunshine JL. Evaluation of breast masses and axillary lymph nodes with [F-18] 2-deoxy-2-fluoro-D-glucose PET. *Radiology.* 1993;187:743–750.
11. Adler LP, Faulhaber PF, Schnur KC, Al-Kasi NL, Shenk RR. Axillary lymph node metastases: screening with [F-18]2-deoxy-2-fluoro-D-glucose (FDG) PET. *Radiology.* 1997;203:323–327.
12. Avril N, Dose J, Jnicke F, et al. Assessment of axillary lymph node involvement in breast cancer patients with positron emission tomography using radiolabeled 2-(fluorine-18)-fluoro-2-deoxy-D-glucose. *J Natl Cancer Inst.* 1996;88:1204–1209.
13. Utech CI, Young CS, Winter PF. Prospective evaluation of fluorine-18 fluorodeoxyglucose positron emission tomography in breast cancer for staging of the axilla related to surgery and immunocytochemistry. *Eur J Nucl Med.* 1996;23:1588–1593.
14. Crippa F, Agresti R, Seregni E, et al. Prospective evaluation of fluorine-18-FDG PET in presurgical staging of the axilla in breast cancer. *J Nucl Med.* 1998;39:4–8.
15. Shreve PD, Steventon RS, Deters EC, Kison PV, Gross MD, Wahl RL. Oncologic diagnosis with 2-[fluorine-18]fluoro-2-deoxy-D-glucose imaging: dual-head coincidence gamma camera versus positron emission tomographic scanner. *Radiology.* 1998;207:431–437.
16. Hoekstra OS, Van Lingen A, Ossenkoppele GJ, Golding R, Teule GJJ. Early response monitoring in malignant lymphoma using fluorine-18 fluorodeoxyglucose single-photon emission tomography. *Eur J Nucl Med.* 1993;20:1214–1217.
17. Mukherji SK, Drane WE, Tart RP, Landau S, Mancuso AA. Comparison of thallium-201 and F-18 FDG SPECT uptake in squamous cell carcinoma of the head and neck. *AJNR.* 1994;15:1837–1842.
18. Martin WH, Delbeke D, Patton JA, et al. FDG-SPECT: correlation with FDG-PET. *J Nucl Med.* 1995;36:988–995.
19. Macfarlane DJ, Cotton L, Ackermann RJ, et al. Triple-head SPECT with 2-[fluorine-18]fluoro-2-deoxy-D-glucose (FDG): initial evaluation in oncology and comparison with FDG PET. *Radiology.* 1995;194:425–429.
20. Holle LH, Trampert L, Lung-Kurt S, et al. Investigation of breast tumors with fluorine-18-fluorodeoxyglucose and SPECT. *J Nucl Med.* 1996;37:615–622.
21. Martin WH, Delbeke D, Patton JA, Sandler MP. Detection of malignancies with SPECT versus PET, with 2-[fluorine-18]fluoro-2-deoxy-D-glucose. *Radiology.* 1996;198:225–231.
22. Mukherji SK, Drane WE, Mancuso AA, Parsons JT, Mendenhall WM, Stringer S. Occult primary tumors of the head and neck: detection with 2-[F-18]fluoro-2-deoxy-D-glucose SPECT. *Radiology.* 1996;199:761–766.
23. Worsley DF, Celler A, Adam MJ, et al. Pulmonary nodules: differential diagnosis using ^{18}F-fluorodeoxyglucose single-photon emission computed tomography. *AJR.* 1997;168:771–774.
24. Strauss LG, Conti PS. The application of PET in clinical oncology. *J Nucl Med.* 1991;32:623–648.
25. Rigo P, Kaschten BJ, Hustinx R, et al. Oncological applications of positron emission tomography with fluorine-18 fluorodeoxyglucose. *Eur J Nucl Med.* 1996;23:1641–1674.
26. Cherry SR, Dahlbom M, Hoffman EJ. 3D PET using conventional multislice tomograph without septa. *J Comput Assist Tomogr.* 1991;15:655–668.
27. Bengel FM, Ziegler SI, Avril N, Weber W, Laubenbacher C, Schwaiger M. Whole-body positron emission tomography in clinical oncology: comparison between attenuation-corrected and uncorrected images. *Eur J Nucl Med.* 1997;24:1091–1098.
28. Imran MB, Kubota K, Yamada S, et al. Lesion-to-background ratio in nonattenuation-corrected whole-body FDG PET images. *J Nucl Med.* 1998;39:1219–1223.
29. Hamberg LM, Hunter GJ, Alpert NM, Choi NC, Babich JW, Fischman AJ. The dose uptake ratio as an index of glucose metabolism: useful parameter or oversimplification? *J Nucl Med.* 1994;35:1308–1312.